J. Fluid Mech. (1998), *vol.* 360, *pp.* 1–20. Printed in the United Kingdom

Particle motion in resonance tubes

By A. GOLDSHTEIN, K. SHUSTER, P. VAINSHTEIN, M. FICHMAN AND C. GUTFINGER

Faculty of Mechanical Engineering, Technion-Israel Institute of Technology, Haifa 32000, Israel

(Received 29 March 1996 and in revised form 29 October 1997)

Small particle motions in standing or travelling acoustic waves are well known and extensively studied. Particle motion in weak shock waves has been studied much less, especially particle motion in periodic weak shock waves which as yet has not been dealt with.

The present study considers small particle motions caused by weak periodic shock waves in resonance tubes filled with air. A simple mathematical model is developed for resonance gas oscillations under the influence of a vibrating piston with a finite amplitude at the first acoustic resonance frequency. It is shown that a symmetrical sinusoidal piston motion generates non-symmetric periodic shock waves. A model of particle motion in such a flow field is suggested. It is found that non-symmetric shock waves cause particle drift from the middle cross-section toward the ends of the resonance tube. The velocity of particle drift is found to be of the order of $D_p\rho_p/T_r\rho_g$, where D_p is the particle diameter, T_r the period of the resonance oscillation, ρ_p and ρ_g are the particle and gas density, respectively. At the same time, the velocity drift strongly depends on the ratio τ/T_r, where τ is the particle relaxation time. Particle drift is vigorous when $\tau/T_r \sim 1$ and insignificant when $\tau/T_r \ll 1$. Theoretical predictions of particle drift in resonance tubes are verified numerically as well as experimentally.

When the particle relaxation time is much smaller than period of the resonance oscillations particles perform oscillations around their equilibrium positions with amplitude of the order of $D_p\rho_p/\rho_g$. It is shown that the difference in oscillation amplitude of particle of difference sizes explains coalescence of aerosol droplets observed in experiments of Temkin (1970).

The importance of the phenomena for particle separation, coagulation and transport processes is discussed.

1. Introduction

This paper analyses the motion of a small rigid particle under the influence of periodic shock waves. Particle transport by periodic shock waves is of practical and theoretical interest. This effect may be applied in the process of cleaning gas of dust.

The separation of small particles with diameters less than 10 μm from a gas stream is fairly difficult. Temkin (1970) has shown that shock waves induced inside a resonance tube can cause rapid coalescence of aerosol particles or droplets. The clusters of particles or larger drops thus produced are significantly easier to separate from the air. Coalescence has been observed for relatively low initial droplet concentrations for which the probability of collisions due to Brownian motion is negligibly small. There are several reasons for particle coalescence under the action of periodic shock waves. One is particle transport along the tube, which may increase particle concentration in certain regions, as well as the probability of particle collisions.

Moreover, since the time-averaged velocity of the particles depends on their sizes, collisions between different-size particles may occur due to their relative motion. Another possible reason for coalescence is significant oscillations of the particles about their equilibrium positions. Simple mathematical models of these phenomena are treated in the present work.

From the theoretical point of view it is interesting to understand why travelling periodic shock waves cause non-periodic particle motions? This question will be answered in the present paper. Drift of small particles under the influence of periodic gas motions is usually connected with standing or travelling acoustic waves. A comprehensive review of particle drift can be found, for example, in Dain *et al*. (1995), or Vainshtein *et al*. (1996). In particular, standing waves cause particle drift to node or antinode wave planes. By analogy, one could expect that particle drift induced by periodic travelling shock waves is caused by the mean gas pressure or velocity gradients inside the resonance tube. Yet the theories of resonance gas oscillation within resonance tubes of Betchov (1956) and Chester (1964) predict a zero average velocity and an undisturbed average pressure.

Goldshtein *et al*. (1996) recently found a higher approximation of the solution of the problem accounting for an averaged pressure gradient along a resonance tube. In particular, it was found that the time-averaged pressure has a minimum (in the section) halfway along the tube. The influence of this pressure non-homogeneity on small particle motion is also considered in the present study.

Another possible reason for particle drift is the influence of a periodic non-symmetrical external force acting on the particle. An example is the vibrotransport of rough inelastic particles by means of a vibrating plate, where non-symmetric oscillations of the plate (see, for example, Blekhman & Dzhanelidze 1964) lead to particle transport not only in the horizontal direction but also in the vertical direction against the action of gravity. In the present study we show that symmetric piston oscillations cause non-symmetric gas oscillations within a resonance tube. There is no complete analogy between the interaction of a particle and a rigid plate, and the interaction between a particle and a shock wave. A mathematical analysis of the latter case is performed in the present study.

2. Problem formulation

The goal of this section is to develop a simple mathematical model of small particle motions in periodic shock waves inside resonance tubes. It is assumed that the particle mass concentration is so small that the influence of the particles on the motion of the gas is negligible. Hence, the gas motion may be treated independently. A simple mathematical model of periodic weak shock wave motion of a 'pure' gas is presented in §2.1. In §2.2 this model is used for the calculation of forces acting on a small particle in such a flow field.

2.1. *Periodic gas motion in a resonance tube*

Particle motion in periodic weak shock waves is generally described by equations of multiphase flow. To simplify the analysis low volume and mass content of the solid phase are assumed, hence the influence of the dispersed phase on fluid motion may be neglected (Nigmatulin 1990). This assumption is fulfilled in the experiments described below. We consider one-dimensional inviscid motion of an ideal gas in a tube restricted at one end by a rigid barrier (plug) and at the other end by an oscillating piston. Let the velocity of the piston be a sinusoidal function of time t with a frequency ω and an

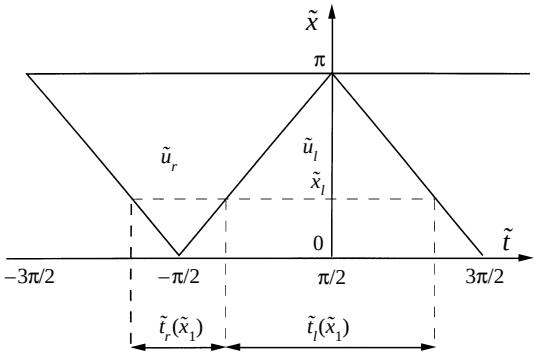

FIGURE 1. The oscillating shock wave.

amplitude u_0. The boundary conditions for this problem may be written in the following form:

$$u(x,t) = 0 \quad \text{at} \quad x = 0, \tag{1a}$$

$$u(x,t) = u_0 \cos \omega t \quad \text{at} \quad x = L + \frac{u_0}{\omega} \sin \omega t, \tag{1b}$$

where $u(x,t)$ is the velocity of the gas, the coordinate x is directed along the tube from the plug to the piston, t is time, and L is the length of the tube. We focus our attention on the case of resonance gas oscillation when the driving frequency, ω, is equal to the first acoustic resonance frequency, ω_r. Numerous experimental treatments of the above problem (see for example Saenger & Hudson 1960; Cruikshank 1972) show that, even for a small driving amplitude, u_0, the gas motion is accompanied by weak shock waves moving back and forth with a frequency, ω_r. For such waves the change of entropy may be neglected and the speed of sound, gas density and pressure are close to their initial values C_0, ρ_0 and P_0, respectively. These values are related by

$$C_0^2 = \gamma \frac{P_0}{\rho_0}, \quad P_0 \rho_0^{-\gamma} = \text{const.} \tag{2}$$

Here γ is the adiabatic exponent and the process is considered isentropic.

The above problem has been treated by several analytical methods. The first consistent analytical results were obtained by Betchov (1956) and Chester (1964) by means of solutions corresponding to standing waves and travelling waves, respectively. Results of both theories coincide when the piston driving frequency, ω, is equal to the resonance frequency, ω_r. Chester's theory has an advantage since it predicts gas oscillation not only for the resonance frequency, as Betchov's theory does, but also in some region close to ω_r. Our recent analysis (see Goldshtein *et al.* 1996) shows that at resonance ($\omega = \omega_r$) both theories yield the correct leading asymptotic term of the order of ε, where $\varepsilon \equiv (u_0/C_0)^{1/2} \quad 1$, and ignore some terms of order ε^2. These neglected terms predict the existence of a mean pressure gradient along the tube. Since a pressure gradient in the gas can, generally speaking, induce motion of small suspended particles, it should also be included in the analysis of the problem. However, simple estimations presented in the following subsection show that the effect of this pressure gradient on the motion of a small particle is minor. Therefore, we limit our model to the leading terms which were obtained by Betchov (1956) and Chester (1964).

A solution of the problem of one-dimensional inviscid motion of an ideal gas under boundary conditions (1) in the resonance case ($\omega = \omega_r = \pi C_0/L$) can be presented in

terms of two standing waves separated by a jump (Betchov 1956; Goldshtein *et al.* 1996). The solution is periodic with the period of the resonant driving oscillation $T_r = 2L/C_0$. All the hydrodynamic properties which characterize the standing waves from the left and from the right of the shock front together with the coordinate of the shock can be expanded in series with respect to the small parameter ε. In the zeroth approximation the speed of the shock wave is equal to the speed of sound, C_0, and the trajectory of the shock front is a zigzag-shaped curve, a fragment of which at the plane $\tilde{x}, \tilde{t}$ is presented in figure 1. The dimensionless variables $\tilde{x}, \tilde{t}$ are defined as follows:

$$\tilde{x} = x\pi/L, \quad \tilde{t} = tC_0\pi/L. \tag{3}$$

In terms of these dimensionless variables the velocity and pressure of the gas can be expressed for one period via the left- and right-hand-side components as follows:

$$u_g(\tilde{t}, \tilde{x}) = \begin{cases} u_r(\tilde{t}, \tilde{x}) & \text{for} \quad -\tilde{x} - \frac{1}{2}\pi \leqslant \tilde{t} \leqslant \tilde{x} - \frac{1}{2}\pi \\ u_1(\tilde{t}, \tilde{x}) & \text{for} \quad \tilde{x} - \frac{1}{2}\pi \leqslant \tilde{t} \leqslant \frac{3}{2}\pi - \tilde{x}, \end{cases} \tag{4a}$$

$$P(\tilde{t}, \tilde{x}) = \begin{cases} P_0 + P_r(\tilde{t}, \tilde{x}) & \text{for} \quad -\tilde{x} - \frac{1}{2}\pi \leqslant \tilde{t} \leqslant \tilde{x} - \frac{1}{2}\pi \\ P_0 + P_l(\tilde{t}, \tilde{x}) & \text{for} \quad \tilde{x} - \frac{1}{2}\pi \leqslant \tilde{t} \leqslant \frac{3}{2}\pi - \tilde{x}, \end{cases} \tag{4b}$$

where

$$u_l(\tilde{t}, \tilde{x}) = u_1 \sin(\tfrac{1}{2}\tilde{x}) \cos(\tfrac{1}{2}\tilde{t} - \tfrac{1}{4}\pi), \quad u_r(\tilde{t}, \tilde{x}) = u_1 \cos(\tfrac{1}{2}\tilde{x}) \sin(\tfrac{1}{2}\tilde{t} - \tfrac{1}{4}\pi), \tag{5a, b}$$

$$P_r(\tilde{t}, \tilde{x}) = -P_1 \sin(\tfrac{1}{2}\tilde{x}) \cos(\tfrac{1}{2}\tilde{t} - \tfrac{1}{4}\pi), \quad P_l(\tilde{t}, \tilde{x}) = -P_1 \cos(\tfrac{1}{2}\tilde{x}) \sin(\tfrac{1}{2}\tilde{t} - \tfrac{1}{4}\pi). \tag{5c, d}$$

Here, u_1, P_1 yield, respectively, half of the maximal velocity and pressure jumps across the shock front

$$u_1 = C_0 A\varepsilon, \quad P_1 = P_0 A\gamma\varepsilon, \tag{6a, b}$$

where the constant A is determined by the ratio of the specific heats γ as follows (see Goldshtein *et al.* 1996):

$$A = \frac{4}{[\pi(\gamma+1)]^{1/2}}. \tag{6c}$$

In the case of gas oscillations at resonance considered here the small parameter ε, which is equal to the square root of the Mach number M, may be expressed via the tube length L and the piston amplitude l as

$$\varepsilon = (\pi l/L)^{1/2}. \tag{7}$$

For any point with the coordinate $\tilde{x}$ the right-hand-side components u_r, P_r of (4) adjacent to the piston are defined in the interval $[\tilde{t}_0(\tilde{x}), \tilde{t}_0(\tilde{x}) + \tilde{t}_r(\tilde{x})]$, while the left-hand-side components u_l, P_l adjacent to the plug are defined in the interval $[\tilde{t}_0(\tilde{x}) + \tilde{t}_r(\tilde{x}), \tilde{t}_0(\tilde{x}) + \tilde{t}_r(\tilde{x}) + \tilde{t}_l(\tilde{x})]$, where

$$t_0(\tilde{x}) = -\tilde{x} - \tfrac{1}{2}\pi, \quad \tilde{t}_r(\tilde{x}) = 2\tilde{x}, \quad \tilde{t}_1(\tilde{x}) = 2\pi - 2\tilde{x}. \tag{8a–c}$$

At a different time the gas velocity and pressure can be obtained from (4) by the periodic continuation

$$u_g(\tilde{t}, \tilde{x}) = u_g(\tilde{t} \pm 2\pi, \tilde{x}), \quad P(\tilde{t}, \tilde{x}) = P(\tilde{t} \pm 2\pi, \tilde{x}). \tag{9}$$

The boundaries of the above time intervals are the times of the shock front transitions through a point with coordinate $\tilde{x}$. Hence, the left-hand-side components u_l, P_l are defined over the period $\tilde{t}_l(\tilde{x})$, while the right-hand-side components u_r, P_r over the period $\tilde{t}_r(\tilde{x})$ (see figure 1). The sum of these periods is independent of the coordinate $\tilde{x}$ and is equal to the dimensionless period of resonant oscillation

$$\tilde{t}_r(\tilde{x}) + \tilde{t}_l(\tilde{x}) = 2\pi. \tag{10}$$

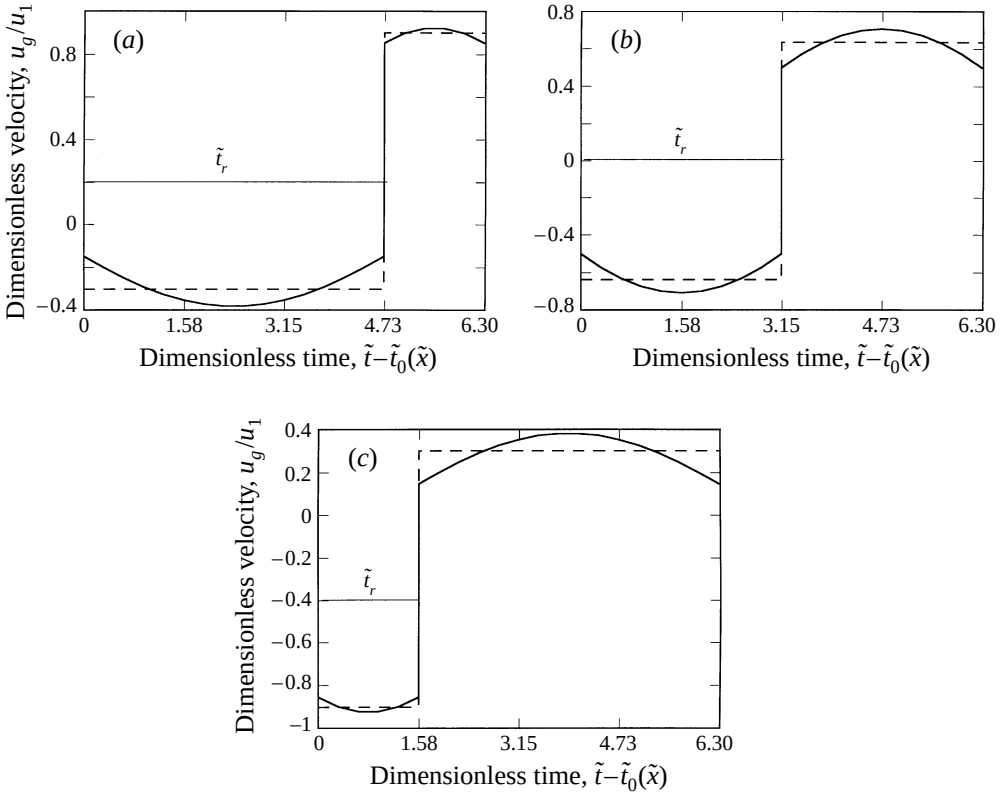

FIGURE 2. Velocity oscillations within resonance tubes: (*a*) three-quarter section ($x = 3L/4$), (*b*) middle section ($x = L/2$), (*c*) quarter section ($x = L/4$). Dashed lines show averaged solution.

In figures 2 and 3 the velocity and pressure, given by (4), are presented in dimensionless form during one cycle at several cross-sections of the resonance tube. It is seen in these figures that the gas velocity and pressure change differently over the period $\tilde{t}_l(\tilde{x})$, $\tilde{t}_r(\tilde{x})$. In order to emphasize this difference we introduce the averaged form of (4). Namely, we average the left- and right-hand components of the solution over the periods $\tilde{t}_l(\tilde{x})$ and $\tilde{t}_r(\tilde{x})$, respectively. For the pressure this procedure obviously yields the initial pressure, while for the velocity we obtain

$$u_{r,\,av}(\tilde{x}) \equiv \frac{1}{\tilde{t}_r(\tilde{x})}\int_{\tilde{t}_o(\tilde{x})}^{\tilde{t}_0(\tilde{x})+\tilde{t}_r(\tilde{x})} u_r(t,\tilde{x})\,\mathrm{d}t, \quad u_{l,\,av}(\tilde{x}) \equiv \frac{1}{\tilde{t}_l(\tilde{x})}\int_{\tilde{t}_0(\tilde{x})+\tilde{t}_r(\tilde{x})}^{\tilde{t}_0(\tilde{x})+2\pi} u_l(t,\tilde{x})\,\mathrm{d}t. \tag{11a, b}$$

Now, equations (4a) and (5a) may be combined with (11a, b) to yield the averaged gas velocity in the form

$$u_{g,\,av}(\tilde{t},\tilde{x}) = \begin{cases} u_{r,\,av}(\tilde{x}) & \text{for} \quad \tilde{t}_0(\tilde{x}) \leqslant \tilde{t} \leqslant \tilde{t}_0(\tilde{x})+\tilde{t}_r(\tilde{x}) \\ u_{l,\,av}(\tilde{x}) & \text{for} \quad \tilde{t}_0(\tilde{x})+\tilde{t}_r(\tilde{x}) \leqslant \tilde{t} \leqslant \tilde{t}_0(\tilde{x})+2\pi, \end{cases} \tag{12}$$

where

$$u_{l,\,av}(\tilde{x}) = u_1\left(\frac{\sin\tilde{x}}{\pi-\tilde{x}}\right), \quad u_{r,\,av}(\tilde{x}) = -u_1\left(\frac{\sin\tilde{x}}{\tilde{x}}\right). \tag{13a, b}$$

This averaged solution for the gas velocity is shown in figures 2 and 3 by the dashed

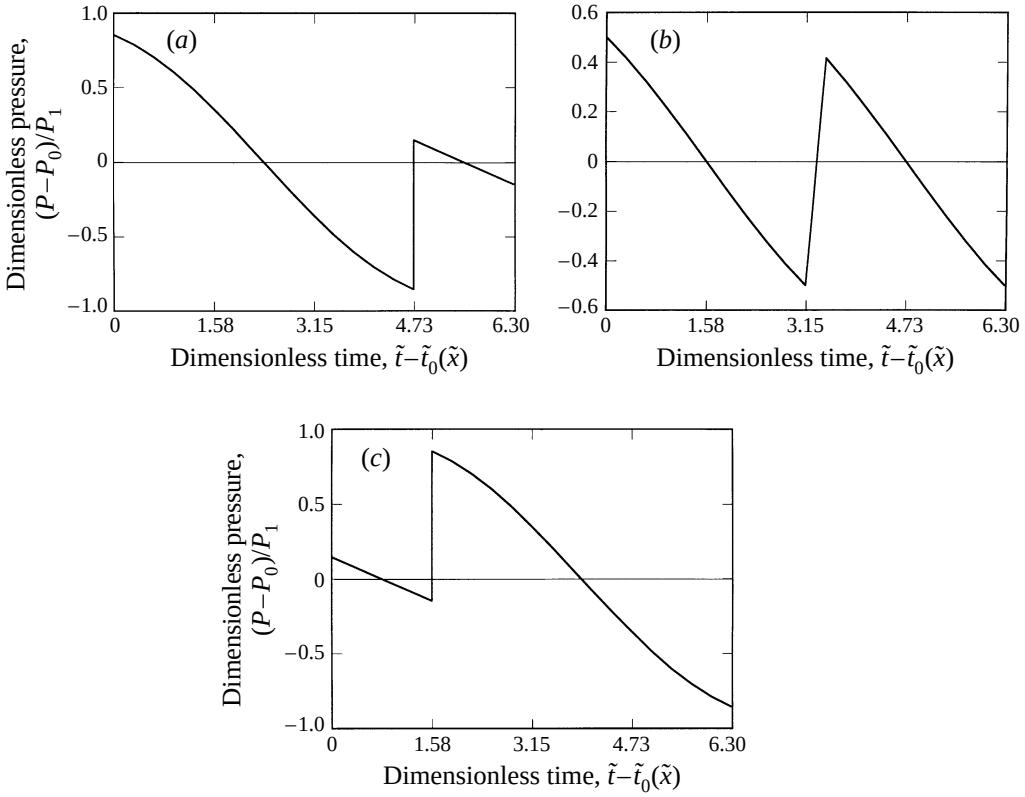

FIGURE 3. Pressure oscillations within resonance tubes: (*a*) three-quarter section ($x = 3L/4$), (*b*) middle section ($x = L/2$), (*c*) quarter section ($x = L/4$). Zero-pressure lines show averaged solution.

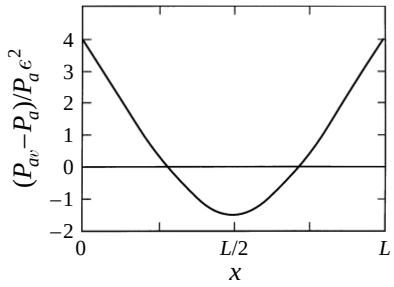

FIGURE 4. Time-averaged pressure distribution.

lines. The solution predicts that in any cross section (except the middle one) the velocity oscillations are described by a non-symmetrical function. The period of oscillation of the gas is the same at any cross section and equal to 2π. However, during some part of the period t_l the gas moves in the positive direction, with the average velocity $u_{l,av}$, while during the remaining part of the period t_r it moves in the negative direction with the average velocity $u_{r,av}$.

As mentioned above, the model of resonant gas oscillations (4), (5) ignores some terms of the order of ε^2. The more exact theory predicts the existence of mean pressure gradients along the tube (see figure 5 of Goldshtein *et al.* 1996). This time-averaged pressure is presented in figure 4. The average pressure at the ends of the tube is higher

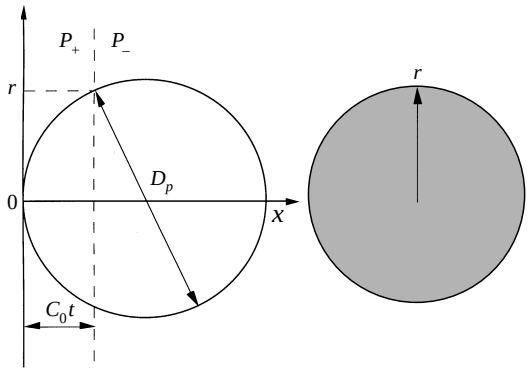

FIGURE 5. Particle cross-section with pressure jump.

than that at its middle. Therefore, one could expect an additional particle drift toward the middle of the tube.

In the following subsection we use the model of gas motion which operates with the averaged values of gas pressure and velocity. The procedure enables us to evaluate interactions between a small rigid particle and a periodic shock wave in relatively simple form.

2.2. *Forces acting on a small particle in a periodic shock wave*

Now we evaluate the forces acting on a small suspended particle induced by viscosity, gravitation, pressure gradient and pressure jump across the shock wave. The last force acts on the particle only at the time when the shock wave passes over the particle. This force is large but its action is very short, hence the influence of this force is estimated from the change in particle velocity. We assume that the particle is a sphere with a diameter D_p, mass m_p, density ρ_p and is moving with a velocity u_p. We first evaluate the force arising from the pressure jump at the shock front. Consider the shock front as a plane with zero thickness which propagates with the velocity C_0. Let the gas pressure ahead of and behind this plane to be constant and denoted as P_+ and P_-, respectively. Then a general relation for the pressure jump across the shock front is $\Delta P = P_+ - P_-$. Simple calculations show that for such conditions the force is the product of the pressure jump and the area, S, of the intersection between the shock plane and the sphere:

$$F_{sh} = \Delta P S, \tag{14}$$

where $S = \pi r^2$ (see figure 5). Now we estimate the effect of this force on particle motion. The equation of particle motion may be written in the form

$$m_p \frac{\mathrm{d}u_p(t)}{\mathrm{d}t} = F_{sh}. \tag{15}$$

Now consider the initial moment $t = 0$ when the shock plane touches the sphere and the x-axis is positive in the direction of shock wave propagation. We neglect the change in particle velocity as compared to the shock wave velocity C_0 and, hence, after the period t the shock front coordinate X_{sh} is equal to tC_0 (see figure 5). During the time it takes the shock wave to travel across the particle diameter, $t_{sh} = D_p/C_0$, the intersection area S is given by

$$S = \pi[(\tfrac{1}{2}D_0)^2 - (\tfrac{1}{2}D_p - C_0 t)^2]. \tag{16}$$

Equations (14)–(16) may be combined to yield the change in particle velocity, Δu_p, due to the pressure jump as

$$\Delta u_p = \int_0^{t_{sh}} \frac{F_{sh}}{m_p} \mathrm{d}t = \frac{\Delta P}{\rho_p C_0}. \tag{17}$$

The drag on bodies, mainly spheres, in unsteady motion in fluids has been the subject of several theoretical and experimental investigations. It is known (Hidy & Brock 1970) that for unsteady slow motion of a sphere in a gas the solution of the Navier–Stokes equations leads to the fluid resistance F in the form

$$F = 3\pi\mu D_p U + \tfrac{1}{12}\pi D_p^3 \phi_g \dot{U} + \tfrac{3}{2} D_p^2 (\pi \rho_g \mu)^{1/2} \int_0^t \frac{\dot{U}(t-\xi)\,\mathrm{d}\xi}{\xi^{1/2}}, \tag{18}$$

where ξ is a dummy variable, $U = u_g - u_p$ is the relative particle velocity and μ is the gas viscosity. The first term of this expression is the steady motion drag, the second term is due to 'added mass' and the third term is the so-called Basset force, which is due to the history of the motion. The influence of unsteadiness on the dynamics and force acting on a particle is determined by the dimensionless group (Nigmatulin 1990)

$$K = \omega d^2/\nu,$$

where ν is the kinematic viscosity. If $K \quad 1$ the second and third terms in (18) are negligible, and the force acting on the particle is determined by the Stokes force. Such a quasi-stationary regime is typical for air suspensions of sufficiently small particles. Note that equation (18) is valid for small Reynolds numbers. However, it follows from an estimate of the order of magnitude of the different terms in the Navier–Stokes equations that condition $K \quad 1$ allows one to neglect the unsteady component of the force exerted by the fluid on the particles for arbitrary Reynolds numbers. In this case the force acting on the particle is entirely determined by the stationary drag. For the particles in the range 1–100 μm and frequencies 68 Hz encountered in Temkin's experiments this parameter in the worse case of 100 μm particles equals 0.2.

In accordance with the generally adopted approach, the drag force for moderate Reynolds numbers should be calculated from an empirical expression. For steady motion the viscous drag force on the sphere is usually expressed in the form

$$F_d = \tfrac{1}{8}\pi D_p^2 \rho_g |U| U C_d(Re), \tag{19}$$

where C_d is a drag coefficient which depends on the Reynolds number,

$$Re = \rho_{gas} D_p U_r/\mu.$$

An expression for C_d as a function of Re may be obtained either from experimental data or numerical calculations. In what follows we use the approximation of Massey (1979)

$$C_d(Re) = \frac{24}{Re}\left(1 + \frac{3}{16} Re\right)^{1/2}. \tag{20}$$

This empirical equation is accurate within several percent for Reynolds numbers smaller than 100.

Experiments on unsteady motions of small particles in fluids show that for moderate Reynolds numbers the steady drag force is the main contributor to the total resistance force. The small difference between steady and unsteady parts is attributed to time changes of the relative gas velocity. In particular, the total drag is larger or smaller than

the steady drag, depending on whether $\dot{U}$ is negative or positive. For several types of unsteady particle motions reasonable models for the total drag accounting for its dependence upon the relative acceleration were suggested by Karanfilian & Kotus (1978) and Temkin & Kim (1980). However, such models are applicable only to the specific unsteady motions for which they were developed and cannot be applied to others. Hence, the present model describing small particle motion in *periodic* weak shock waves is limited only to cases for which equations (19) and (20) apply.

For completeness we should estimate the other forces acting on the particle, namely the gravity force, F_g and the force F_{gr} due to the pressure gradient in the gas surrounding the particle. In the case of one-dimensional motion considered here the absolute values of these forces may be written in the form

$$|F_g| = \tfrac{1}{6}\pi D_p^3 \rho_p g, \tag{21}$$

$$|F_{gr}| = \tfrac{1}{6}\pi D_p^3 \left|\frac{\partial P}{\partial x}\right|, \tag{22}$$

where g is the acceleration due to gravity.

To assess the relative magnitude of these forces we consider the data of Temkin (1970). In his case the resonance tube was 250 cm long and of 7.62 cm internal diameter. When the piston was oscillated at the first fundamental resonant frequency a maximal shock strength of about $0.1P_0$, was produced, where P_0 is the atmospheric pressure. Setting $\gamma = 1.4$ and $C = 340$ m s^{-1} for the air and using (6*a–c*) one obtains $\varepsilon = 0.024$ and $u_1 = 12.1$ m s^{-1}. The aerosol particles were droplets of oleic acid vapour produced on salt nuclei of size in the range 1–10 μm. Setting $\rho_g = 1.29$ kg m^{-3}, $U \sim u_1$ and $\mu = 18.2 \times 10^{-6}$ kg ms^{-1} one obtains Reynolds numbers in the range 1.72–17.2. For such Reynolds numbers expression (19) is applicable. Therefore, to estimate the ratio of the gravity and drag forces we should use equations (19) and (21) to yield the ratio

$$\left|\frac{F_g}{F_d}\right| = \frac{2D_p \rho_p}{3U_r^2 \rho_g C_d}, \tag{23}$$

which for the density ratio $\rho_p/\rho_g = 1000$ yields $|F_g/F_d| < 0.002$.

Using (21) and (22) we obtain the ratio of the pressure gradient force and the gravity force in the form

$$\left|\frac{F_{gr}}{F_g}\right| = \left|\frac{\partial x}{\rho_p g}\right|. \tag{24}$$

According to figure 4 the average pressure drop over a half-length of the tube is $5.5P_0\varepsilon^2$. Therefore, assuming $|\partial P/\partial x| \sim 11P_0\varepsilon^2/L$ for the pressure gradient we obtain

$$\left|\frac{F_{gr}}{F_g}\right| \sim \left|\frac{11P_0\varepsilon^2}{\rho_p g L}\right| \approx 0.022.$$

From the above estimations it follows that for typical experimental conditions the gravity force (21) and the pressure gradient force are negligibly small in comparison with the drag force (19).

Now we estimate the change of particle velocity Δu_p due to the shock wave. Setting $\Delta P = 0.1P_0$ into equation (17) one obtains $\Delta u_p \approx 1/34$ m s^{-1}. This value is much smaller than the characteristic value of the particle velocity which is of the order of u_1. Hence, we drop Δu_p from our considerations and assume that the particle velocity changes continuously.

The main result of the present analysis indicates that the motion of a small particle in a weak periodic shock wave may be described by the equation

$$m_p \frac{\mathrm{d}u_p(t)}{\mathrm{d}t} = F_d. \tag{25}$$

Here the drag force F_d is given by equations (19) and (20), $U = u_{g,av}(\tilde{t}, \tilde{x}) - u_p(t)$ is the relative particle velocity and $u_{g,av}(\tilde{t}, \tilde{x})$ is given by equations (12) and (13).

The solution (25) is treated in the following section by means of a semi-analytical model. A more elaborate model of the motion of a small particle which is based on equations (5*a*, *b*) is treated numerically in §4.

3. Solution of the equation of motion of a small particle in a periodic shock wave

In this section we solve the equation of motion of a small particle under the influence of a non-symmetric periodic weak shock wave. In §3.1 an analytical solution of this problem is derived for the special case of spatially uniform oscillations. In §3.2 this solution is extended to the motion of a small particle inside a resonance tube.

3.1. *The spatially uniform case*

We consider the periodical motion of a gas with a period $T = t_1 + t_2$. During the time t_1 the gas moves with a constant velocity U_1 in the positive direction, while during t_2 it moves with a constant velocity U_2 in the negative direction, i.e.

$$u_g(t) = \begin{cases} U_1 & \text{for} \quad 0 \leqslant t \leqslant t_1 \\ U_2 & \text{for} \quad t_1 \leqslant t \leqslant T, \end{cases} \qquad u_g(t) = u_g(t+T). \tag{26}$$

The motion described by (26) is shown schematically in figure 6. We restrict our analysis to the case for which the average gas displacement per period is equal to zero, i.e.

$$U_1 t_1 + U_2 t_2 = 0. \tag{27}$$

The motion of the gas as described by equations (26) and (27) accounts for the change in the direction of the gas velocity with time analogously to (12) though it ignores its spatial variation. In this special case the problem can be solved analytically. We introduce dimensionless relative particle velocity u_d and time t_d by the relations

$$u_d = UD_p \rho_g / \mu, \quad t_d = t/\tau, \tag{28a, b}$$

where $U = U_i - u_p(t)$ $(i = 1, 2)$ is the relative particle velocity and $\tau = \rho_p D_p^2/(18\mu)$ is the time of particle velocity relaxation. Equations (19), (20) and (25) may now be combined to yield

$$\frac{\mathrm{d}u_d(t_d)}{\mathrm{d}t_d} = -u_d(t_d)\,(1 + \tfrac{3}{16} u_d(t_d))^{1/2}. \tag{29}$$

A general solution of (29) may be written in the form

$$u_d(t_d) = \frac{64c \exp(-t_d)}{3[c - \exp(-t_d)]^2}, \tag{30}$$

where c is an arbitrary constant.

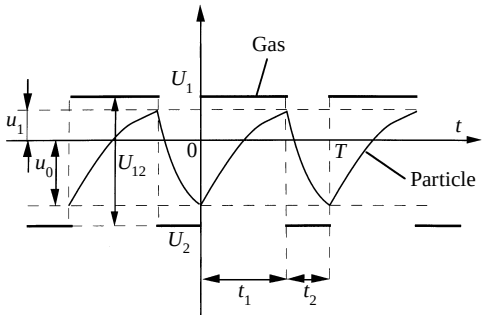

FIGURE 6. Schematic of periodic particle motion induced by a periodic shock wave. Bold straight lines indicate gas velocity, curves correspond to particle velocity.

Now we use equations (26) and (27) to formulate the mathematical problem of particle motion in a periodic shock wave. We make several assumptions which will be verified *a posteriori*. We first assume that the particle velocity u_p is a periodic function with the same period T as that of the gas oscillations, i.e.

$$u_p(t) = u_p(t+T). \tag{31}$$

Without any loss of generality we choose as the initial moment $t = 0$ the one when the shock wave propagating in the positive direction approaches the particle which has a velocity u_0. Since we neglect the velocity jump of the particle due to the pressure drop across the shock wave we take the initial condition as (see figure 6)

$$u_p(0) = u_0. \tag{32}$$

We assume that the relative particle velocity at the moment $t = 0$ is positive. Substitution of (30) into condition (32) yields the following condition for constant $c = c_1$ (say):

$$c_1 = \frac{(1+3u_{d0}/16)^{1/2}+1}{(1+3u_{d0}/16)^{1/2}-1}, \tag{33a}$$

where

$$u_{d0} \equiv u_d(0) = (U_1 - u_0)\, D_p \rho/\mu. \tag{33b}$$

In terms of this parameter the above assumption may be written

$$u_{d0} > 0. \tag{33c}$$

During the period t_1 when the gas moves with velocity U_1 the constant c_1 determines the particle velocity as prescribed by (28*a*):

$$u_p(t_d) = \frac{U_1 D_p \rho_g}{\mu} - \frac{64 c_1 \exp(-t_d)}{3[c_1 - \exp(-t_d)]^2} \quad \text{for} \quad 0 \leqslant t_d \leqslant t_{d1} = t_1/\tau. \tag{34}$$

After the time t_1, when the shock wave propagating in negative direction reaches the particle, the speed of the particle is (see figure 6)

$$u_p(t_{d1}) = u_1. \tag{35}$$

We assume that the relative particle velocity at the moment t_1 is negative. This assumption together with (28*a*) allow us to determine constant c_2 in (30) in the form

$$c_2 = \frac{(1+3u_{d1}/16)^{1/2}+1}{(1+3u_{d1}/16)^{1/2}-1}, \tag{36a}$$

where
$$u_{d1} \equiv -u_d(t_{d1}) = (u_1 - U_2)\, D_p \rho_g / \mu. \tag{36b}$$

In terms of this parameter the latter assumption may be written

$$u_{d1} > 0. \tag{36c}$$

During the period t_2 when the gas moves with velocity U_2 the constant c_2 determines the particle velocity prescribed by (28*a*) as

$$u_p(t_d) = \frac{U_2 D_p \rho_g}{\mu} + \frac{64 c_2 \exp(t_{d1} - t_d)}{3[c_2 - \exp(t_{d1} - t_d)]^2} \quad \text{for} \quad t_{d1} \leqslant t_d \leqslant T/\tau. \tag{37}$$

Equations (34) and (37) describe the motion of the particle during the period T. These equations are determined except for the two unknown constants c_1 and c_2 which depend on the particle velocity at the moments $t = 0$ and $t = t_1$. In order to obtain two additional conditions for these constants we take into account the fact that particle velocity is a continuous function which satisfies the condition of periodicity (31). Therefore, the following matching conditions should be imposed:

$$u_{d0} = \frac{U_{12} D_p \rho_g}{\mu} - \frac{64 c_2 \exp(-t_2/\tau)}{3[c_2 - \exp(-t_2/\tau)]^2}, \tag{38a}$$

$$u_{d1} = \frac{U_{12} D_p \rho_g}{\mu} - \frac{64 c_1 \exp(-t_1/\tau)}{3[c_1 - \exp(-t_1/\tau)]^2}, \tag{38b}$$

where $U_{12} = U_1 - U_2$.

We have obtained a system of four equations (33*a*), (36*a*), (38*a*, *b*) for the four constants u_{d0}, u_{d1}, c_1 and c_2. Generally speaking, this system can be solved only numerically, but for several special cases it can be treated asymptotically.

Consider the case when both times t_1 and t_2 are much larger than the time of particle relaxation, τ:

$$t_1 \quad \tau, \quad t_2 \quad \tau. \tag{39}$$

Then, $\exp(-t_1/\tau) \quad 1$, $\exp(-t_2/\tau) \quad 1$ and the solution of the above system may be written in the form

$$u_{d0} = U^{(0)} - U^{(1)} \exp(-t_2/\tau), \quad u_{d1} = U^{(0)} - U^{(1)} \exp(-t_1/\tau), \tag{40a, b}$$

$$c_1 = c^{(0)} + c^{(1)} \exp(-t_2/\tau), \quad c_2 = c^{(0)} + c^{(1)} \exp(-t_1/\tau), \tag{40c, d}$$

where

$$U^{(0)} = U_{12} D_p \rho_g / v, \quad c^{(0)} = \frac{(1 + 3U^{(0)}/16)^{1/2} + 1}{(1 + 3U^{(0)}/16)^{1/2} - 1}, \tag{41a, b}$$

$$U^{(1)} = 64/(3c^{(0)}), \quad c^{(1)} = \frac{64}{3U^{(0)}[1 + 3U^{(0)}/(16\mu)]^{1/2}}. \tag{41c, d}$$

One can see from (40*a*, *b*) and (41*a*, *b*) that u_{d0}, u_{d1} are positive. This proves our previous assumptions (33*c*,) (36*c*). On the other hand, the existence of solution (41) guarantees the existence of the periodical solution (34), (37), (28*b*).

Now consider particle displacement in the positive and negative directions, respectively,

$$\Delta x_{p1} \equiv \int_0^{t_1} u_p(t)\, \mathrm{d}t, \quad \Delta x_{p2} \equiv \int_{t_1}^{T} u_p(t)\, \mathrm{d}t. \tag{42}$$

Substitution of the solution given by (34) and (37) into (42) and integration yields

$$\Delta x_{p1} = U_1 t_1 + \frac{32\rho_p D_p}{27\rho_g}\left[\frac{c_1}{c_1 - \exp(-t_1/\tau)} - \frac{c_1}{c_1 - 1}\right], \tag{43a}$$

$$\Delta x_{p2} = U_2 t_2 - \frac{32\rho_p D_p}{27\rho_g}\left[\frac{c_2}{c_2 - \exp(-t_2/\tau)} - \frac{c_2}{c_2 - 1}\right]. \tag{43b}$$

The average particle displacement and speed of transportation during the period may be defined as

$$\Delta x_p = \Delta x_{p1} + \Delta x_{p2}, \quad V_p = \Delta x_p / T. \tag{44a, b}$$

Substitution of (43*a*, *b*) into (44*a*) gives

$$\Delta x_p = \frac{32\pi_p D_p}{27\rho_g}\left[\frac{C_1}{C_1 - \exp(-t_1/\tau)} - \frac{C_1}{C_1 - 1} - \frac{C_2}{C_2 - \exp(-t_2/\tau)} + \frac{C_2}{C_2 - 1}\right]. \tag{45}$$

It follows from (45) and (44*b*) that the average particle displacement and velocity during one period are of the order $D_p\rho_p/\rho_g$ and $D_p\rho_p/T_r\rho_g$, respectively. The dependence of Δx_p and V_p on the dynamic characteristics of the external oscillations are hidden in the expression in the square brackets in (45). To illustrate the character of this dependence we consider the small-Reynolds-number approximation (40*c*, *d*). Substitution of this approximation into (45) allows Δx_p, V_p to be estimated as small values of the order of $\exp(-t_1/\tau) + \exp(-t_2/\tau)$. Since for small Reynolds numbers $\tau \quad T$ both exponents are negligibly small and, hence, the drift is negligible. We show in the following section that for moderate Reynolds numbers, when the time of particle relaxation is of the order of the period of the resonance oscillations, $\tau \approx T_r$, the drift caused by periodic weak shock waves is quite vigorous.

3.2. *Motion of a small particle inside a resonance tube*

In this section we extend the simple model for a spatially uniform case to the motion of a small particle inside a resonance tube. The solution is then tested on the experimental data reported by Temkin (1970). For simplicity, we assume that the displacement of a small particle during a single period is negligible, and velocity gradients in the gas have no effect on the motion of the particle. Under these circumstances the problem of particle motion can be posed for any cross-section independently. This means that the problem of averaged particle motion in any cross-section of a resonance tube may be reduced to the spatially uniform case treated above.

In order to describe the motion of a small particle at a given cross-section of the resonant tube it is necessary to prescribe the times t_1, t_2 and velocities U_1, U_2 which together with equations (26) and (27) completely determine the motion of the gas as a function of the coordinate x. To do that we use the model of the average motion of the gas given by equations (8), (12), (13), and define

$$t_2 = T_r \tilde{t}_r(\tilde{x})/2\pi = T_r x/L, \quad t_1 = T_r \tilde{t}_l(\tilde{x})/2\pi = T_r(1 - x/L), \tag{46a, b}$$

$$U_1 = u_{l,av}(\tilde{x}) = u_1 \frac{\sin(\pi x/L)}{\pi(1 - x/L)}, \quad U_2 = u_{r,av}(\tilde{x}) = -u_1 \frac{\sin(\pi x/L)}{(\pi x/L)}. \tag{46c, d}$$

Expressions (46) for t_1, t_2, U_1, U_2 are substituted into equations (33*a*), (36*a*) and (38*a*, *b*). The closed system of four equations is solved numerically for Temkin's experimental data and for the particle diameters $D_p = 15$, 25, 50 and 100 μm. As a result the parameters c_1, c_2 are obtained as functions of x. These functions are

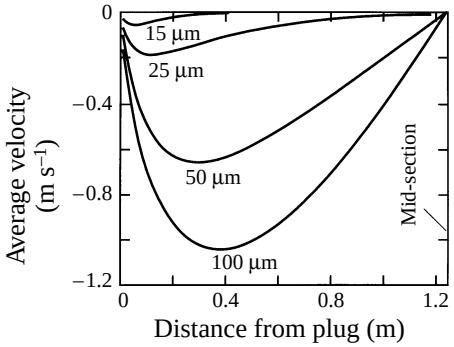

FIGURE 7. Particle drift velocity as a function of distance from plug for different particle diameters, calculated for Temkin's experiments.

combined with equations (44*a*, *b*) to yield average particle velocities V_p and displacements in the positive direction Δx_{p1} during the period T_r. Figures 7 and 8 show the drift velocity V_p and displacement Δx_{p1} of a small particle versus distance from the plug for the half of the tube $x < L/2$. For the other half of the resonance tube the velocity may be obtained by antisymmetric continuation, and the displacement by symmetric continuation.

Figure 7 shows that particles of all sizes are transported from the tube mid-section to the plug. All average (drift) particle velocities along the tube have the common feature of being equal zero at the mid-cross-section $x = L/2$ and at the section $x = 0$ (at the rigid plug). At $x = L/2$ the velocity vanishes because it is antisymmetric with respect to this point, while at $x = 0$ it vanishes because the plug is impenetrable. In each cross-section the average particle velocity increases with particle diameter. The maximum particle drift velocity is about 1 m s^{-1} for a particle of 100 μm. This value is of the order of the scaling factor $D_p \rho_p / T_r \rho_g$ in equation (44*b*). As mentioned above, such an order of particle drift velocity may be attained only when the period of resonance oscillations T_r is of the order of the particle relaxation time τ. Indeed, $T_r/\tau \approx 0.5$ for $D_p = 100$ μm. The decrease of the average particle velocity with its diameter seen from figure 7 is explained by the decrease of the scaling factor and of the ratio T_r/τ. Because of this, particles with small ratio $\tau/T_r \quad 1$ will drift significantly only in a small part of the resonance tube where $t_1/\tau \sim 1$ or $t_2/\tau \sim 1$. For example, for particles with diameter $D_p = 15$ μm the drift takes place in a part of the resonance tube of the length about 0.2 m (see figure 7).

Figure 8 shows particles displacements in the positive direction per a single period versus the distance from the plug. One can see that for any cross-section the displacement decreases with increasing of the particle diameter D_p. This tendency is explained by the particle inertia which is characterized by the particle relaxation time τ. The smaller the particle diameter the smaller particle relaxation time and, as a result, the smaller the differences between the particle and the gas displacement (dashed curve in figure 8). Particle displacements, unlike gas displacement, are maximal in the middle section and equal to zero at the plug (i.e. at $x = 0$). It follows from figure 8 that for the relatively large particles with $D_p \geqslant 25$ μm the displacement Δx_{p1} is a non-monotonic function of x. This effect is explained by the particle inertia.

For the small enough particles (in our case for $D_p \leqslant 15$ μm) displacement Δx_{p1} change monotonically (see the curve in figure 8 for $D_p = 15$ μm) and hence the drift phenomenon is insufficient. Particles oscillate around their initial position with amplitude Δx_{p1}. However, even so, collisions take place between different small

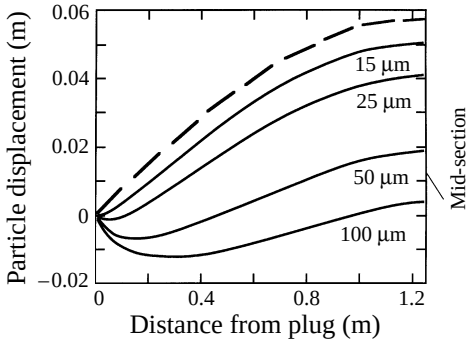

FIGURE 8. Amplitude of particle displacement as a function of distance from plug for different particle diameters, for Temkin's experiments. The dashed curve shows the gas displacement.

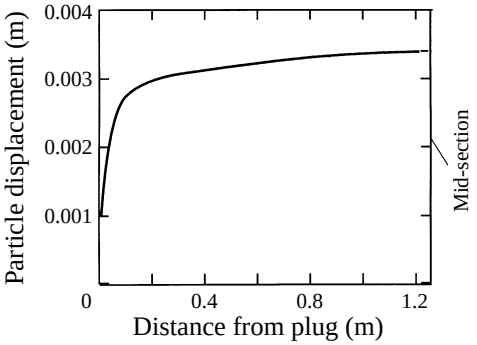

FIGURE 9. Difference in displacements of 1 μm particles relative to that of 10 μm particles for Temkin's experimental conditions.

particles. The reason is that particles of different sizes oscillate with different amplitudes because of the difference in the relaxation times. Figure 9 shows the difference between displacements Δx_{p1} of particles with diameters of 1 and 10 μm, respectively. These values of particle diameters characterize the smallest and largest particles in Temkin's experiment. It follows from figure 9 that differences in oscillation amplitude between these smallest and largest particles exceed 0.34 cm within the resonance tube except in a small region close to the plug. These differences in amplitudes are much larger than the average initial distance between the particles, which is of the order of $N_0^{-1/3} \approx 0.05$ cm, where $N_0 \approx 10^4$ cm^{-3} is the initial number concentration in Temkin's experiments. Therefore, one can expect frequent collisions between particles in the range 1–10 μm which lead to coagulation of particles with different diameters.

We now compare the ability of sound waves to cause particle agglomeration with that of shock waves. For such a goal we estimate particle relative displacements induced by periodic acoustic waves *vis-à-vis* weak shock waves. Temkin (1994) estimates that under the influence of acoustic waves particle relative displacement is not larger than the amplitude of gas oscillations, which is of the order of several hundreds of a micrometre. On the other hand, our estimations have now shown that weak shock waves under typical conditions cause relative particle displacements of the order of several millimetres. Hence, the relative particle displacement in a weak shock wave is an order of magnitude larger than that in an acoustic waves. The particle relative displacement is a important parameter which characterizes the ability of aerosol

particles to collide and, consequently, to agglomerate. Since weak shock waves produce significantly larger relative particle displacements than acoustic waves, the weak shock waves will be more effective in agglomerating low-concentration aerosols.

4. Numerical and experimental studies of particle drift in a resonance tube

The analysis presented above is based on a number of approximations. These approximations can affect the model accuracy and should be justified. In this section theoretical predictions of particle drift in resonance tubes are verified numerically as well as experimentally. Each of these methods has its own advantages and disadvantages. Experiments provide information about actual particle behaviour. However, the measurement of rapid motion of a small particle requires rather sophisticated equipment and facilities suitable for conducting precise experiments (see for example Temkin & Kim 1980). Unfortunately, the latter were not at our disposal, and our experiments are rather crude by modern standards.

The qualitative results reported here were obtained with relatively large and heavy particles which can be readily observed by means of an ordinary video camera. For such particles the gravity force cannot be neglected. Experiments with these particles cannot be used directly to validate the present model. Nevertheless, they may be used to demonstrate the existence of the drift phenomenon.

4.1. *Numerical study of particle drift in a resonance tube*

The model presented in this paper uses time-averaging of gas flow and particle motion and assumes locally uniform flow, while neglecting gravity. The time-averaging of the gas flow is performed over the time intervals $\tilde{t}_r$ and $\tilde{t}_l$, respectively, see (11). The time-averaging of the motion of the particle is done over the period of gas oscillation, see (44). The numerical solution allows the errors caused by each of the assumptions of the semi-analytical model to be estimated, as well as the total accuracy of the model. The model chosen for the numerical solution is the one based on Chester's equations (5*a*, *b*) for the velocity of the gas.

We now examine the effect of time-averaging of gas oscillations for the spatially homogeneous case (see §3.1). For this purpose the two variants of equation (25) which use different models for the motion of the gas are employed. Two examples, shown in figure 2(*c*) are solved: the one shown by the dashed lines uses the time-averaged model, while that shown by the solid lines uses Chester's model.

Numerical calculations were performed for a particle initially at rest. The results indicate that after several periods of gas oscillations the velocity of the particle changes periodically with the same period as that of the gas. The numerical results during the first few periods of oscillations for the two models that describe the drift of 100 μm particles are compared in figure 10(*a*, *b*) with the predictions of the semi-analytical solution.

Figure 10(*a*) displays the time-averaged model of gas oscillation, while figure 10(*b*) corresponds to Chester's model. The figure shows the displacement as a function of time, for a drifting particle initially at $x = L/4$. The semi-analytical solution of (45), shown on the plots as straight lines, describes the average motion of the particle, i.e. particle drift, while the numerical solution, depicted by the wavy lines, shows the actual motion of the particle at any instant of time. As seen in figure 10(*a*), the averaged drift long the tube as calculated from the semi-analytical model is practically the same as that computed numerically. Figure 10(*b*) is equivalent to 10(*a*), except for the model, which is now that of Chester, shows once again that the average drift obtained

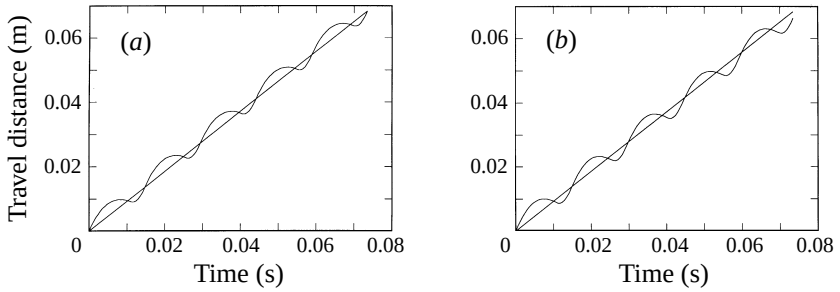

FIGURE 10. Particle drift in periodic spatially-homogeneous shock waves for 100 μm particles: (*a*) the time-averaged model of gas motion, (*b*) Chester's model. Straight lines: average motion from semi-analytical theory; wavy lines: actual motion from the numerical calculation.

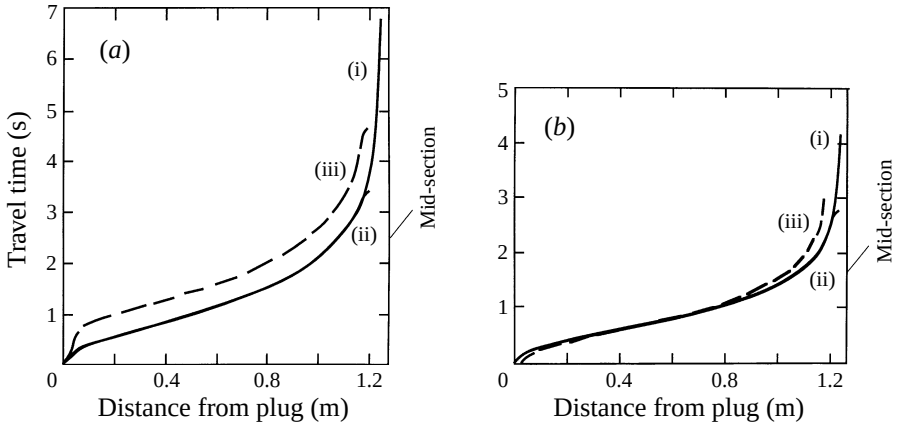

FIGURE 11. Travel time as a function of the initial particle distance from the plug, as calculated from the semi-analytical model (i), and the numerical solution in the absence (ii) and presence of gravity (iii). (*a*) $D_p = 50$ μm, (*b*) $D_p = 100$ μm.

analytically is close to that predicted by the numerical calculations. Here (45) slightly overestimates the average particle drift, with the error not exceeding 3 %.

Figure 11 (*a*, *b*) shows the drift of 50 μm and 100 μm particles, respectively, in a resonance tube with the parameters of that of Temkin. The numerical calculations have shown that in the absence of gravity a particle which begins its motion anywhere along the tube always reaches the plug. In upward vertical motion in the presence of gravity the particle may stop somewhere along the tube before reaching the plug.

Computations show that a particle of a given size, no matter where it starts its motion, always stops at the same distance from the plug. The further the initial position from the stopping point, the longer the travel time and vice versa. Thus, a particle initially located at the stopping point, will stay there, and its travel time will, obviously, be zero. Figure 11 (*a*, *b*) presents the particle travel time as a function of its initial distance from the plug. The distance corresponding to zero time denotes the stopping point for a given particle. Hence, the total travelling distance of a particle is found by subtracting the distance of the stopping point from the initial distance of the particle from the plug.

The numerical and analytical models for the zero gravity case are marked on the plots as (i) and (ii), respectively. One can see that both solutions based on the time-averaged and Chester's gas flow models yield very similar results everywhere, except close to the mid-section.

In order to estimate the effect of gravity on particle drift, the gravity term was introduced into equation (25) and the equation solved numerically for the entire tube domain $0 < x/L < 0.5$. Results of the numerical computations are presented in figure 11(*a*, *b*) by the lines marked as 3 (iii). Since the gravity force acts in the direction opposite to drift, this force reduces particle drift, resulting in particles stopping before reaching the plug. For 50 μm particles (figure 11*a*) the gravity force significantly reduces the drift velocity (increases the travel time) of the particle, yet the stopping point is very close to the plug. On the other hand figure 11(*b*) indicates that for the faster drifting 100 μm particles (see figure 7) the travel time is very close to that without gravity, and curves 2 and 3 almost coincide, except in the vicinity of the plug and the mid-section. In this case the stopping point is at a larger distance from the plug than in the case of 50 μm particles.

Figure 11 also indicates that the effect of gravity is most pronounced at tube locations where the drift velocity is lowest, i.e. near the plug or the mid-section (see figure 7).

In general the numerical results are rather close to the analytical solutions, and indicate that the analytical approach presented in this paper has considerable merit.

4.2. *Experimental study of particle drift in a resonance tube*

An experiment has been designed in order to show the existence of particle drift under the influence of a periodic shock wave. The apparatus used consists of a vibrating piston inside a vertical tube, 365 cm long and 5.4 cm in internal diameter. The tube is closed at one end by a rigid plug and at the other by the piston, which is driven sinusoidally by a vibrator. The vibrator imposes oscillations on the piston of a fixed amplitude of about 2.2 cm, with frequencies continuously varying within the range 1–100 Hz. When the frequency of the oscillations is far from the first resonance frequency, $f_r \sim 46.6$ Hz, the resulting sound waves are distorted but continuous. However, when the frequency is close to f_r, weak shock waves, of about 0.3 atm strength, are registered.

A hook is inserted horizontally through a hole drilled in the tube, and a light polystyrene-foam spherical particle of 3.5 mm in diameter is suspended from the hook by means of a string. The string extends to the part of the tube where the theory predicts high particle drift velocities (see figure 7). In the absence of gas motion the particle hangs on the string, as in figure 12(*a*). In the presence of gas motion, the particle moves under the action of the acoustic and shock waves. The motion of the particle is recorded by a video camera. The positions of the particle at different times are measured from the recorded image. The camera provides 25 frames per second with an exposure time of 1/4000 s, allowing the exact position of the particle at time intervals of 1/25 s to be measured.

The video tape shows that the acoustic waves cause very weak particle oscillations, with the particle oscillating like a pendulum close to its equilibrium position. However, when shock waves appear in the tube rapid upward particle motion is registered. The particle moves very quickly from its lowest to its uppermost position (see figure 12*b*) and oscillates around it.

The average particle velocity may be calculated by dividing the distance between the bottom and top positions and the time needed for traversing this distance. Taking this time interval from the video tape and setting the distance as twice the length of the string, the average particle velocity may be calculated. In our experiments the change from lowest to highest particle positions occurred between two consecutive frames, hence the velocities are in excess of 2 m s^{-1}. Such relatively high velocities were needed

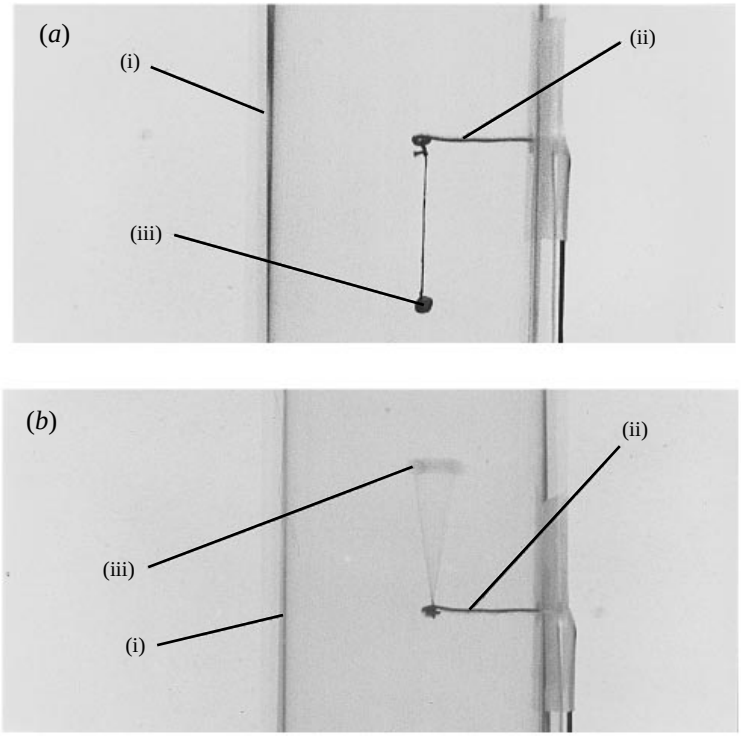

FIGURE 12. Particle positions (*a*) in the absence and (*b*) in the presence of shock waves. Notation: (i) resonance tube, (ii) bracket, (iii) particle.

to affect our very large particle. Unfortunately, our equipment was not accurate enough to allow monitoring the motion of really small particles. Still, the phenomenon of particles drifting under the influence of periodic shock waves, as described in the present paper, has been demonstrated.

5. Conclusions

The present paper describes particle drift under the influence of periodic shock waves. This is an interesting phenomenon hitherto not reported in the literature. This phenomenon has now been predicted analytically, computed numerically and verified experimentally. It opens new areas of applied research on particle separation and concentration.

The present study can also be applied to particle agglomeration. Comparing the present results with those of particle agglomeration under the influence of acoustic waves (Temkin 1994), we note that shock waves cause much larger relative particle displacements, leading to more enhanced agglomeration.

This research was supported by the Fund for the Promotion of Research at the Technion, and by the Israel Science Foundation Grant no. 529-93-1. A.G. acknowledges the support of the Gileadi Program.

REFERENCES

Betchov, B. 1958 Non-linear oscillations of the column of a gas. *Phys. Fluids* **1**, 205–212.

Blekhman, I. I. & Dzhanelidze, D. G. 1964 *Vibratsionnoe Peremeshthenie* (Vibrational transport). Nauka, Moscow (in Russian).

Chester, W. 1964 Resonant oscillations in closed tubes. *J. Fluid Mech.* **18**, 44–64.

Cruikshank, D. B. 1972 Experimental investigation of finite-amplitude acoustic oscillations in a closed tube. *J. Acoustic Soc. Am.* **52**, 1024–1036.

Dain, Y., Fichman, M., Gutfinger, C., Pnueli, D. & Vainshtein, P. 1995 Dynamics of suspended particles in a two-dimensional high-frequency sonic field. *J. Aerosol Sci.* **26**, 4, 575–594.

Goldshtein, A., Vainshtein, P., Fichman, M. & Gutfinger, C. 1996 Resonance gas oscillations in closed tubes. *J. Fluid Mech.* **322**, 147–163.

Hidy, G. M. & Brock, J. R. 1970 *The Dynamics of Aerocolloidal Systems*. Pergamon.

Karanfilian, S. K. & Kotus, T. J. 1978 Drag on a sphere in unsteady motion in liquids at rest. *J. Fluid Mech.* **87**, 85–96.

Massey, B. S. 1979 *Mechanics of Fluids*. Pergamon.

Nigmatulin, R. I. 1990 *Dynamics of Multiphase Media*. Annals of Nuclear Energy, Hemisphere, Washington.

Saenger, R. A. & Hudson, G. E. 1960 Periodic shock waves in resonating gas columns. *J. Acoustic, Soc. Am.* **32**, 961–971.

Temkin, S. 1970 Droplet agglomeration in a shock wave flow field. *Phys. Fluids* **13**, 1639–1641.

Temkin, S. 1994 Gasdynamic agglomeration of aerosols. I. Acoustic waves. *Phys. Fluids* **6**, 2294–2303.

Temkin, S. & Kim, S. S. 1980 Droplet motion induced by weak shock waves. *J. Fluid Mech.* **96**, 137–157.

Vainshtein, P., Fichman, M., Shuster, K. & Gutfinger, C. 1996 Centerline particle concentration in a wave tube. *J. Fluid Mech.* **306**, 31–42.